8.6

A THREE-DIMENSIONAL CLOUD MODELING STUDY ON THE DYNAMICAL AND MICROPHYSICAL VARIABILITY OF THUNDERSTORMS IN DIFFERENT CLIMATE REGIMES

Robert E. Schlesinger, Shane A. Hubbard and Pao K. Wang
Department of Atmospheric and Oceanic Sciences
University of Wisconsin – Madison
Madison, Wisconsin 53706
USA

1. INTRODUCTION

Several regions of the world from upper midlatitudes to the Tropics are subject to thunderstorms. Aside from the United States, they include western Europe (Ludlam 1963), the Caucasus region of Russia (Sulakvelidze et al. 1977), northern India (Ramaswamy 1956), Indonesia (Sukanto 1969), Central America (Portig 1976), and the south and north coasts of Australia as well as the uplands of east equatorial and southeast Africa (Court and Griffiths 1982). The number of thunderstorm days per annum is especially high in the overland tropical regions just noted (Court and Griffiths 1982), especially Indonesia (Sukanto 1969).

Even within the confines of the United States, warm-season severe thunderstorms can occur in a wide variety of synoptic flow patterns, geographical locations, and vertical profiles of temperature and relative humidity (e.g., Fawbush and Miller 1954, Beebe 1955; Johns 1984; Dunn and Horel 1994).

An evolving research group at the University of Wisconsin, led by third author Wang, has for over 15 years been studying the microphysical structure of warm-season thunderstorms in different climatic regions of the earth as documented in Straka (1989), Johnson et al. (1993, 1994), Lin and Wang (1997), and Lin et al. (2005; henceforth LWS05). The key tool has been a three-dimensional (3D) cloud model known as WISCDYMM (the Wisconsin Dynamical and Microphysical Model), originated by Straka (1989), subsequently modified by the research group (Johnson et al. 1993, 1994; Lin and Wang 1997; LWS05), and summarized briefly in section 2.

However, these previous case studies with WISCDYMM have been limited to one semi-arid midlatitude region (the U.S. High Plains) and the humid subtropics. Straka (1989) simulated a Colorado multicell storm, Johnson et al. (1993, 1994) analyzed the impact of ice microphysics on a Montana supercell, and Lin and Wang (1997) simulated a multicell storm in Taipei, Taiwan. Most recently, by means of six 2-h WISCDYMM simulations, LWS05 compared the microphysical aspects of three summertime thunderstorms apiece in the High Plains (the Colorado and Montana cases plus a North Dakota storm) and the humid subtropics (the Taipei storm and two south Florida cases).

Despite being limited to only two climatic regions, the studies listed in the last two paragraphs yielded two notable findings:

a) The fraction of the total condensate mass contributed by each hydrometeor type seemed to be quasi-steady throughout the active life of a given storm after its early adjustment phases, as was also true for the individual microphysical transfer rates contributing to the production and depletion of each precipitating hydrometeor category; and

b) The partitioning showed contrasting breakdowns in one geographic region versus the other. Thus, in LWS05, the Montana storm had a higher frozen fraction of condensate mass than the Taipei storm, ~82% versus ~57%, while the other High Plains storms had mass partitionings similar to the Montana case and the Florida storms more nearly resembled the Taipei case in that regard. Since the simulated storm structures were found to compare favorably with observations (LWS05), it is quite plausible to regard them as physically realistic.

The above findings motivated us to embark on a subsequent WISCDYMM-based thunderstorm variability study that is still evolving. This project is in much the same overall spirit as in LWS05, but subsumes a much larger number of thunderstorm cases, distributed among a wider variety of climatic zones, and includes a sizable minority of extratropical cases from seasons other than summer. This substantially wider variety of storm cases, vis-à-vis LWS05, has been compiled in order to investigate whether or not systematic differences in bulk microphysical characteristics of simulated storms in contrasting climatic regions continue to apply when the variety of thunderstorm-supporting environments is thus broadened. This paper highlights some of the results we have obtained to date.

**Corresponding author address:* Robert E. Schlesinger, Department of Atmospheric and Oceanic Sciences, University of Wisconsin - Madison, Madison, Wisconsin, 53706; e-mail: schlesin@meteor.wisc.edu.

2. EXPERIMENTAL CONDITIONS

2.1 *Model Properties*

WISCDYMM is a time-dependent nonhydrostatic quasi-compressible 3D model in standard Cartesian coordinates. The model domain is 55x55x20 km^3 in the respective x-, y- and z-coordinates, with 55x55x100 grid cells of dimensions 1.0x1.0x0.2 km^3. Finite-difference advection schemes and boundary conditions are as in LWS05, with subgrid flux parameterizations as in Straka (1989). Radiation, topography and the Coriolis force are omitted. The time step is 2 s, with a reduced sound speed of 200 m s^{-1}.

Predicted model fields are the three wind components, potential temperature, water vapor mixing ratio, and the mixing ratios for five classes of hydrometeors: cloud water, cloud ice, rain, snow and graupel/hail. The microphysical package features a bulk parameterization which, as elaborated in Straka (1989), is based mainly on Lin et al. (1983) and Cotton et al. (1982, 1986). Cloud water droplets and cloud ice crystals are monodisperse and move with the air, while precipitating hydrometeors follow inverse exponential size distributions.

The bulk microphysics parameterization provides for up to 37 transfer rates, several of which (e.g., condensation onto and evaporation from wet snow and wet graupel/hail) are turned off in the simulations reported herein. Most importantly for this paper, 25 of the active transfer rates are a source or sink of precipitation. The symbolic names and physical meanings of all active sources and sinks for each of the three precipitation classes are listed in Table 1.

2.2 *Initialization*

As in Klemp and Wilhelmson (1978), convection in WISCDYMM is initiated by an ellipsoidal buoyant bubble in the lower central portion of the domain, superimposed on a horizontally homogeneous hydrostatic base state. The bubble is 10 km in radius and 4 km deep, centered 2 km above ground level (AGL), with a maximum excess potential temperature of 4.5C at its center. The water vapor mixing ratios in the bubble are adjusted to keep the relative humidity equal to its base-state value.

In each case, the base state is computed by vertically interpolating the temperature, dewpoint and horizontal wind components from the closest available sufficiently deep rawinsounding in space and time on the University of Wyoming's sounding archive website *http://weather.uwyo.edu/upperair/sounding.html* to the model grid levels, every 100 m because the model grid is staggered. The hydrostatic base state pressure is integrated upward starting from the archived surface pressure. The relative humidity and water vapor mixing ratio, depending on the temperature T, are based on saturation with respect to (w.r.t.) liquid water if $T > 0^{\circ}C$ and w.r.t. ice if $T \leq -20^{\circ}C$ with a gradual transition in between.

2.3 *Environmental Lifting Option*

If in a given case WISCDYMM produces a storm that dissipates unrealistically early, such as a single short-lived (~1 h or less) cell in a situation where a multicell system lasting 2 h or longer occurred, there may be insufficient moisture in the lowest few kilometers to truly represent the actual near environment of the observed storm.

In such instances, prior to imposing the buoyant bubble, the vertical temperature and mixing ratio profiles in the interpolated sounding are preprocessed for higher relative humidities by imposing a time-independent parabolic lifting profile between 0 and 4 km AGL, maximized at 10 cm s^{-1} at 2 km AGL, using a 300-s time step for 1 or 2 or 3 h, whichever duration is sufficient to generate a system that persists for 2 h or better. The only processes operating during lifting are vertical advection and, if any supersaturation occurs, an instantaneous saturation adjustment that releases latent heat and drops out any resulting condensate while keeping the surface temperature and mixing ratio unchanged. Cases for which 3 h of lifting do not suffice are discarded.

2.4 *Range of Experiments Performed*

Some 60 WISCDYMM storm simulations have either been run or are in progress, initialized with University of Wyoming archive rawinsoundings from various parts of the world. Most locations are in western European countries and the United States east of the Rockies, but there is also a more limited sampling from other regions such as Australia and southeast Asia. As of this writing, 48 simulations have been completed and microphysically postprocessed.

To avoid excessive length, our scope herein is limited to 28 of the 48 completed and postprocessed simulations. Table 2 lists the 25 sounding locations (three of which were used for two simulations apiece out of the 28) by city and state (or country, if other than the United States), call symbol, latitude, longitude and elevation. The soundings are grouped by each of several climatic zones within which the locations fall on a worldwide climatic classification map in Moran and Morgan (1994), further subdividing their "temperate continental" classification subjectively into "warm summer" and "cool summer" subtypes. Despite being located as far north as southern Minnesota, the two European stations Nimes (France) and S Pietro di Capofiume (Italy) are evidently considered subtropical because they have a Mediterranean climate with mild winters for their latitudes.

Each of the 28 storm cases is listed in Table 3 by a symbolic name and various parameters relating to its

initial base-state profile on the model grid after interpolation from the associated sounding and modification of the lowest 4 km by lifting, if any. Note the following points with regard to Table 3:

1) The symbolic case name embodies the location, date and time of the associated sounding, starting with the station call symbol (Table 2) and continuing with the year, month, day and hour, e.g., 11722 020716-12 for the Brno, Czech Republic on 16 July 2002 at 1200 UTC.

2) The tabulated parameters are duration of lifting (absent in eight cases), surface elevation ZSFC, surface temperature TSFC, mean boundary-layer water vapor mixing ratio QVBL, lifting condensation level LCL, convective available potential energy CAPE, convective inhibition CIN, bulk Richardson number BRN, lifted index LI, Total Totals index TOTL, and melting level ZMLT.

3) ZSFC and TSFC are taken from the raw archived sounding, while the subsequent parameters pertain to its preprocessed counterpart on the WISCDYMM grid. Parameters QVBL through TOTL are computed the same way as in the archive except for CAPE, whose calculation ignores latent heat of fusion in the archive but takes it into account in our study, resulting in higher CAPE by typical margins of ~20-40% in the eight cases without lifting.

4) Whereas all six storm cases in LWS05 fell within the summer months of June through August (for the Northern Hemisphere), eight of our 23 extratropical cases occurred in spring or fall among the warm-summer temperate continental, humid subtropical and dry-summer subtropical climate zones. Partly for that reason, there are sizable spreads among the values of CAPE, LI and TOTL in those climatic regions.

5) The five cases from the humid Tropics are more consistent with one another, with modest LI and TOTL values and high or very high ZMLT levels as well as high QVBL values, though CAPE shows a large spread of CAPE between the Darwin and Calcutta profiles.

2.5 *Run-Time Strategy*

Each WISCDYMM simulation is run out to 120 min (2 h), restarting every 20 min while saving the model fields and auxiliary microphysical data every 2 min. During any one 20-min segment, the domain is translated at a constant velocity relative to the earth so as to aim the most interesting convective cell for an ending position near the center of the domain area. The translation velocity generally varies among segments, and a segment is rerun if the first attempt ends with the cell of interest insufficiently well centered.

3. RESULTS

3.1 *Storm Types and Updraft Intensities*

A capsule summary of mature storm strength and structure for the 28 simulated storms is displayed in Table 4. This table shows the largest and smallest spatial maxima of the updraft velocity during 80-120 min, well after the storm has adjusted from the overshooting updraft peak at ~15 min in response to the vigorous initial buoyant bubble. Also included is a thumbnail description of the storm type on the basis of Tecplot animations of an isosurface we have empirically found to be a reasonable approximation to the cloud boundary at most levels, the 90% isosurface for the relative humidity w.r.t. ice (RHi),

Not surprisingly, Table 4 shows large percentage spreads of both temporal updraft velocity extrema, strongest for the temperate continental case ILX 040714-00 and weakest for the humid tropical case WSSS 000918-09. Twenty cases were judged to be multicellular, eight of them "backbuilding" (new cells form in the quadrant of an existing storm opposite to the direction of prominent anvil blowoff) and the other 12 "complex" (new cells form in two or more quadrants of an existing storm). The remaining eight cases, none of them tropical, were judged to be supercellular, with cell splitting in seven cases and a late transition to backbuilding multicellular in three of those.

Joint perusal of Tables 3 and 4 shows, as one might anticipate, that environments with CAPE < 2000 J kg^{-1} produce weaker mature storm updrafts than environments with CAPE > 3000 J kg^{-1}, although updraft magnitudes also vary widely at intermediate CAPE values, e.g., RKJJ 010714-12 versus BMX 980409-00. Also, storm environments with BRN > 50 yield multicellular storms, and BRN ≤ 50 for all eight supercells. This is consistent with findings from the classic idealized storm simulation study of Weisman and Klemp (1982). However, relatively low BRN values need not imply supercellular behavior, because five of the simulated storms with BRN < 50 are multicellular.

3.2 *Hydrometeor Mass Partitionings*

As in LWS05, we evaluated and intercompared the overall microphysical makeup of our simulated storms by computing time-averaged masses for the five individual hydrometeor (condensate) classes for the five constituent classes (cloud water, cloud ice, rain, snow, graupel/hail) and five combinations among them over a large part of the mature storm stage, then dividing each of the 10 resulting mass magnitudes by the time-averaged total condensate mass. The five combined indices, as in LWS05, represent total ice (cloud ice, snow and graupel/hail), total liquid (100% minus total ice), total precipitation (rain, snow and graupel/hail), total cloud (100% minus total precipitation) and frozen precipitation (snow and graupel/hail). The time-averaging spanned 60-120 min in all storm simulations.

Table 5 displays the resulting percentage mass indices for the 28 storm cases. Large case-to-case variability of each index is immediately apparent, especially between the five tropical cases and the remaining ones, but also among the six warm-summer temperate continental cases and among the ten subtropical cases.

Thus, total ice among all cases ranges from ~20% in the tropical case VECC 000722-00 to ~77% in the temperate continental case ILX 040714-00 and the boreal case WSE 000715-00. But it also ranges between ~41% and ~77% among the warm-summer temperate continental cases and between ~39% and ~74% among the subtropical cases, or nearly two-thirds the total spread among all 28 cases.

These findings differ from those of LWS05, who reported on the whole considerably less variability of most mass indices among either their three High Plains storms or among their three humid subtropical storms than between a storm in one region and a storm in the other. In LWS05, to the nearest percentage point, total ice was 78-82% for the High Plains cases versus 48-57% for the humid subtropical cases. Analogous ranges for the High Plains versus humid subtropical cases for individual hydrometeor classes were 7-9% versus 8-14% for cloud water, 6-9% versus 4-5% for cloud ice, 11-13% versus 32-38% for rain, 24-36% versus 14-18% for snow, and 37-49% versus 30-36% for garupel/hail.

Several interesting points emerge when we compare some of our partitionings with those in LWS05:

1) Among our five humid tropical cases, YPDN 021104-12 is comparable to the humid subtropical cases in LWS05, but the other four cases have far less cloud ice, graupel/hail, total ice and frozen precipitation and much more cloud water.

2) Among our six warm-summer temperate continental cases, ILX 040714-00 is largely comparable to the High Plains cases in LWS05, while OKX 050915-12 has a higher percentage of rain and lower ice-related indices of all types than any of the humid subtropical cases therein. These extreme examples strongly suggest that which climatic region a storm occurs in can at times be trumped by the presence of an atypical airmass for the region and/or time of year. Case ILX 040714-00 had the highest CAPE and TOTL indices and the most unstable LI of all 28 cases (Table 3) and also the strongest mature updraft (Table 4), circumstances that tend to favor a severe storm with abundant hail aloft if not at the ground, even though the boundary layer was far more humid and the melting level far higher than for a typical High Plains summertime environment. To a smaller extent, this is also true for the dry-summer subtropical case LFME 030817-12 from southern France. Case OKX 050915-12, by contrast, was largely a non-severe heavy rain event that occurred in an entrenched unseasonably humid airmass of marine tropical origin with far more modest values of the same indices (Table 3), producing a correspondingly weaker updraft (Table 4).

3) In two April cases from the humid subtropical zone, both in the southeastern United States (BMX 980409-00 and BNA 980416-18), most of the mass indices are solidly intermediate between the High Plains and humid subtropical cases of LWS05. Although humid air from the Gulf of Mexico occupied the lowest 3 km, the soundings from midlevels on up were considerably colder than for a typical summertime subtropical sounding (and both observed storm situations spawned major tornadoes).

4) Despite being located at a much lower latitude than any of the High Plains soundings in LWS05, our Tucson sounding TUS 980718-00 supported a model storm with mass indices comparable to those for their High Plains storms. This cannot be explained by high CAPE, a very unstable LI or a low melting level ZMLT, since none of these are present in the sounding (Table 3). A much more plausible contributing factor is the very high LCL, much farther above ground than in any of our other 27 cases and less than 1 km below the melting level (Table 3), implying a cold cloud base even though the surface is hotter than in any of our other cases.

5) The temperate oceanic case 07145 970824-1200 from northern France has mass indices largely comparable to those of the subtropical cases in LWS05, although no clear reason emerges from Tables 3 and 4.

3.3 *Precipitation Source/Sink Rankings*

In this subsection, we highlight a subset of seven storms out of the 28 in order to obtain some idea of whether the presence of several notably high or low hydrometeor mass indices is associated with atypical rankings among some of the more important sources and sinks of precipitation, and also whether these rankings differ significantly between storms with and without exceptional mass indices.

Within the ranges of the mass indices among the 28 cases, five of these seven selected storms show several extreme values in Table 5:

1) Humid tropical case VECC 000722-00 is lowest or second lowest for all five ice indices (cloud ice, snow, graupel/hail, total ice, frozen precipitation), the highest rain index, the second highest cloud water index, and the second lowest total precipitation index.

2) Humid tropical case YPDN 020314-00 is second lowest for all ice indices except cloud ice and also has the lowest total precipitation index and the highest cloud water and total cloud indices.

3) Subtropical dry-summer case 40179 021016-00 is quite high in ice fractions for total ice and frozen precipitation, and has the highest graupel/hail index.

4) Humid tropical case WSSS 000918-09, while less extreme than the preceding three storms, has the lowest cloud ice fraction and also has low fractions of graupel/hail, total precipitation and frozen precipitation.

5) Temperate continental warm-summer case ILX 040714-00 has the highest frozen precipitation fraction and second highest fractions of both total ice and graupel/hail, along with the second lowest cloud water fraction.

In contrast to the five cases above, all the mass indices fall in the middle of their ranges for the remaining two storms in the subset, subtropical dry-summer case LGAT 020727-12 and temperate oceanic case 07145 970824-12.

To include a quick look at the cloud structure for the seven storms highlighted in this subsection, Figs. 1-7 show pseudo-3D Tecplot frames of their approximate cloud boundaries as viewed looking northward at 60 and 90 min. One is a splitting supercell (40179 021016-00, Fig. 3), two are backbuilding multicells (VECC 000722-00, Fig. 1; ILX 040714-00, Fig, 5), and the remaining four among them are complex multicells (YPDN 020314-00, Fig. 2; WSSS 000918-09, Fig. 4; LGAT 020727-12, Fig. 6; 07145 970824-12, Fig. 7), although the differences between the two types of multicellular structure are less apparent from these snapshots than from Tecplot animations of the full life cycles of the storms.

One other more vexing limitation of the Tecplot displays is that, as noted in subsection 3.1, we have thus far been using the 90% RHi isosurface as a proxy for the cloud boundary, Because Tecplot treats the volume enclosed by the isosurface.(RHi > 90%) as hollow instead of solid, the viewing field can be whited out at model levels where RHi exceeds 90% over a sufficiently large portion of the domain area. This deficiency is apparent in Figs. 1, 2, 4 and 5, in which the apparent cloud base is ~3 km AGL despite LCL's well below 1 km AGL in each of the four cases shown in those figures (Table 3).

For each of the three classes of precipitation in WISCDYMM, Table 6 displays for these seven storms the rankings of the individual sources and sinks of each precipitation class as 60-120 min time-averaged fractions of the total production and depletion respectively, analogously to LWS05. The more important a source or sink, the lower the number assigned to its rank in Table 6. Thus, the most important contributor is assigned a ranking of 1, the second most important a ranking of 2, etc.

Despite the large microphysical contrasts between the very low ice fraction indices in the three humid tropical cases (VECC 000722-00, YPDN 020314-00 and WSSS 000918-09) and the high ice fraction indices in cases ILX 040714-00 and 40179 021016-00, and the absence of any notably high or low indices in cases LGAT 020727-12 and 07145 970824-12, the only two storms of the seven to show any atypical source/sink rankings among our 28 experiments are cases VECC 000722-00 and YPDN 020314-00. These two cases are distinctive because they are among the only three out of the 28 in which accretion of cloud water by rain (qracw) ranks #1 rather than #3 among the rain sources, and VECC 000722-00 is the only case for which accretion of cloud water by snow (qsacw) ranks #1 ahead of Bergeron snow growth from cloud ice (qisfi) instead of vice versa. However, at least among the various contributors of rank 3 or better, none of the other five cases in the subset of seven show any atypical rankings even though one of them has low ice fractions (WSSS 000918-09) and two of them have high ice fractions (ILX 040714-00, 40179 021016-00).

Finally, it is of interest to briefly compare some of the more important (lower numbered) rankings in Table 6 with results from LWS05, the main point being that some rankings that discriminated between the summertime High Plains and humid subtropical storms in LWS05 do not discriminate among different climate zones in our broader study, at least for the four climatic regions sampled among our subset of seven cases. In each comparison, LWS05 reported rankings that discriminated between their two climate zones but which correspond to their humid subtropical storms for our entire subset. Among rain sinks, evaporation (qrcev) ranked #1 for the High Plains cases versus #2 for the subtropical cases, but #2 throughout our subset. Analogous contrasts between LWS05 and our study apply to accretion of rain by hail (qhacr) as a rain sink (#2 for the High Plains cases versus #1 for the subtropical cases in LWS05, #1 throughout our subset), and also to accretion of rain by hail (qhacr) as a hail source (#2 or #3 for the High Plains cases versus #1 for the subtropical cases in LWS05, #1 throughout or subset).

4. ACKNOWLEDGMENTS

The thunderstorm simulations reported herein are based on research partially supported by National Science Foundation (NSF) Grants ATM-0234744 and ATM-0244505. Any findings or opinions expressed in this paper are those of the authors and do not necessarily reflect the views of NSF.

5. REFERENCES

Beebe, R. G., 1955: Types of airmasses in which tornadoes occur. *Bull. Amer. Meteor. Soc.*, **36**, 349-350.

Cotton, W. R., M. A. Stevens, T. Nehrkorn, and G. J. Tripoli, 1982: The Colorado State University three-dimensional cloud/mesoscale model - 1982. Part II: An ice phase parameterization. *J. Rech. Atmos*., **16**, 295-320.

_____, G. J. Tripoli, R. M. Rauber, and E. A. Mulvihill, 1986: Numerical simulations of the effects of varying ice crystal nucleation rates and aggregation processes on orographic snowfall. *J. Climate Appl. Meteor.*, **25**, 1658-1680.

Court, A., and J. F. Griffiths, 1982: Thunderstorm Climatology. In *Thunderstorms: A Social, Scientific and Technological Documentary*, Vol. 2, E. Kessler, Ed., U. S. Department of Commerce, 11-52.

Dunn, L. B., and J. D. Horel, 1994: Prediction of central Arizona convection. Part I: Evaluation of the NGM and Eta model precipitation forecasts. *Wea. and Forecasting*, **9**, 495-507.

Fawbush, E. J., and R. C. Miller, 1954: The types of airmasses in which North American tornadoes form. *Bull. Amer. Meteor. Soc.*, **35**, 154-165.

Johns, R. H., 1984: A synoptic climatology of northwest flow severe weather outbreaks. Part II: Meteorological parameters and synoptic patterns. *Mon. Wea. Rev.*, **112**, 449-464.

Johnson, D. E., P. K. Wang, and J. M. Straka, 1993: Numerical simulations of the 2 August 1981 CCOPE supercell storm with and without ice microphysics. *J. Appl. Meteor.*, **32**, 745-759.

_____, _____, and _____, 1994: A study of microphysical processes in the 2 August 1981 CCOPE supercell storm. *Atmos. Res.*, **33**, 93-123.

Klemp, J. B., and R. B. Wilhelmson, 1978: The simulation of three-dimensional convective storm dynamics. *J. Atmos. Sci.*, **35**, 1070-1096.

Lin, H.-M., and P. K. Wang, 1997: A numerical study of microphysical processes in the 21 June 1991 northern Taiwan mesoscale precipitation system. *Terres. Atmos. Ocean. Sci.*, **4**, 385-404.

_____, _____, and R. E. Schlesinger, 2005: Three-dimensional nonhydrostatic simulations of summer thunderstorms in the humid subtropics versus High Plains. *Atmos. Res.*, **78**, 103-145.

Lin, Y.-L., R. D. Farley, and H. D. Orville, 1983: Bulk parameterization of the snow field in a cloud model. *J. Climate Appl. Meteor.*, **22**, 1065-1092.

Ludlam, F. H., 1963: Severe local storms - A review. *Severe Local Storms. Meteor. Monogr.*, **5**, No. 27, Amer. Meteor. Soc., 1-30.

Moran, J. M., and M. D. Morgan, 1994: *Meteorology: The atmosphere and the science of weather*, 4th ed. Macmillan College Publishing Company, New York, 517 pp.

Portig, W. H., 1976: The Climate of Central America. In *Climates of Central and South America*, World Survey of Climatology, Vol. 12, Elsevier, New York, 81-133.

Ramaswamy, C., 1956: On the sub-tropical jet stream and its role in the development of large-scale convection. *Tellus*, **8**, 26-60.

Straka, J. M., 1989: *Hail Growth in a Highly Glaciated Central High Plains Multi-Cellular Hailstorm*. Ph. D. thesis, Department of Meteorology, University of Wisconsin - Madison, 413 pp.

Sukanto, M., 1969: Climate of Indonesia. In *Climates of Northern and Eastern Asia*, World Survey of Climatology, Vol. 8, Elsevier, New York, 215-229.

Sulakvelidze, G. K., N. I. Glushkova, and L. M. Fedchenko, 1977: *Forecasting of Hail, Thunderstorms and Showers*. Keter Publishing House, Jerusalem, 150 pp.

Weisman, M. L., and J. B. Klemp, 1982: The dependence of numerically simulated convective storms on vertical wind shear and buoyancy. *Mon. Wea. Rev.*, **110**, 504-520.

TABLE 1. Sources and sinks of precipitation in the WISCDYMM bulk microphysics parameterization.

Symbolic representation	Description of process
qrcev	Evaporation of rain
qhsbv	Sublimation of hail
qssbv	Sublimation of snow
qhdpv	Deposition to hail
qsdpv	Deposition to snow
qscni	Autoconversion of cloud ice to snow
qsaci	Accretion of cloud ice by snow
qraci	Accretion of cloud ice by rain
qsfi	Bergeron growth of snow from cloud ice
qhaci	Accretion of cloud ice by hail
qracw	Accretion of cloud water by rain
qsacw	Accretion of cloud water by snow
qrcnw	Autoconversion of cloud water to rain
qhacw	Accretion of cloud water by hail
qsfw	Bergeron growth of snow from cloud water
qhmlr	Melting of hail
qsmlr	Melting of snow
qhshr	Shedding from hail
qiacr	Accretion of rain by cloud ice
qrfrz	Freezing of rain
qsacr	Accretion of rain by snow
qhacr	Accretion of rain by hail
qracs	Accretion of snow by rain
qhcns	Autoconversion of snow to hail
qhacs	Accretion of snow by hail

TABLE 2. Locations of the rawinsoundings adapted for initialization of the 28 storm cases alluded to in the text, showing relevant information adapted from the University of Wyoming archive and Moran and Morgan (1994).

City and state/country	Call symbol	Latitude (˚)	Longitude (˚)	Elevation (m)	Climatic zone
Lincoln, IL*	ILX	+40.2	-89.3	178	Temperate continental, warm summer
Albany, NY	ALB	+42.7	-73.8	96	"
Upton, NY	OKX	+40.8	-72.9	20	"
Beijing, China	ZBAA	+39.9	+116.2	55	"
Sterling, VA	IAD	+39.0	-77.4	93	"
Brno, Czech Republic	11722	+49.1	+16.8	300	Temperate continental, cool summer
Lindenberg, Germany	10393	+52.2	+14.1	115	"
Poprad, Czech Republic	11952	+49.0	+20.3	706	"
Trappes, France	07145	+48.8	+2.0	168	Temperate oceanic, cool summer
Essen, Germany	10410	+51.4	+7.0	153	"
Tucson, Arizona	TUS	+32.1	-110.0	779	Dry/desert
Birmingham, AL	BMX	+33.2	-86.7	178	Subtropical, humid
Nashville, TN	BNA	+36.2	-86.5	210	"
Kwangju AFB, South Korea	RKJJ	+35.1	+126.8	13	"
Fort Worth, TX	FWD	+32.8	-97.3	171	"
Athens, Greece	LGAT	+37.9	+23.7	15	Subtropical, dry summer
Changsha, China	ZGCS	+28.2	+113.0	46	"
Nimes, France	LFME	+43.9	+4.4	62	"
Bet Dagan, Israel	40179	+32.0	+34.8	35	"
S Pietro de Capofiume, Italy	16144	+44.6	+11.6	11	"
Trapani, Italy	LICT	+37.9	+12.5	14	"
Stony Plain, Canada	WSE	+53.5	-114.0	766	Boreal
Singapore, Malaysia*	WSSS	+1.4	+103.9	16	Tropical humid, wet
Darwin, Australia*	YPDN	-12.4	+130.8	30	Tropical humid, wet and dry
Calcutta, India	VECC	+22.6	+88.4	6	"

*More than one thunderstorm case for this location.

TABLE 3. Selected environmental parameters for each of the 28 selected storm cases.

Case	Lifting (h)	ZSFC (m)	TSFC (˚C)	QVBL (g/kg)	LCL (m AGL)	CAPE (J/kg)	CIN (J/kg)	BRN	LI (C˚)	TOTL (C˚)	ZMLT (m AGL)
ILX 960420-00	0	178	22.2	13.30	601	2420	-4	29.1	-7.0	56.4	3159
ALB 950715-00	2	96	32.6	17.52	1293	3997	-40	294.3	-6.4	52.4	4920
ILX 040714-00	1	178	26.8	18.87	675	4835	-11	20.5	-11.3	62.2	4400
OKX 050915-12	1	20	23.6	17.05	276	1892	-4	107.3	-4.2	46.2	4172
ZBAA 050710-12	0	55	30.2	13.64	1485	1692	-37	63.9	-4.3	49.0	4003
IAD 940501-00	1	93	22.2	13.71	680	1770	-12	32.9	-4.2	49.0	3613
11722 020716-12	2	300	29.0	12.45	1260	1742	-13	27.0	-4.7	51.7	3785
10393 020710-18	1	115	31.8	10.28	2280	1389	-27	104.8	-4.2	55.8	3891
11952 050731-12	1	706	28.0	11.84	1454	2061	-4	46.4	-6.0	55.6	3464
07145 970824-12	1	168	31.2	12.87	1564	1955	-16	105.1	-4.0	50.7	3648
10410 040717-12	2	153	26.8	10.63	1424	1102	-3	54.0	-3.9	53.3	3220
TUS 980718-00	0	779	38.2	9.35	3274	1222	-2	44.6	-3.4	54.7	4050
BMX 980409-00	1	178	21.0	14.57	487	2314	-21	12.7	-7.6	59.0	3892
BNA 980416-18	0	210	20.2	13.35	416	1463	-10	19.0	-6.2	55.2	3354
RKJJ 010714-12	0	13	28.4	19.32	620	2433	-9	28.2	-5.6	45.6	5006
FWD 010615-00	1	171	32.4	17.28	1308	4717	-7	166.5	-10.1	58.8	4431
LGAT 020727-12	2	15	29.6	13.98	984	2662	-6	364.2	-6.6	50.4	3726
ZGCS 040421-12	1	46	30.2	15.37	1382	2665	-39	50.0	-5.0	48.3	4341
LFME 030817-12	2	62	29.4	16.41	959	4312	0	104.6	-9.0	54.6	3910
40179 021016-00	1	35	20.2	13.81	514	2254	-22	25.6	-5.5	51.8	3604
16144 980630-12	2	11	30.4	13.26	1364	2278	-3	20.2	-8.0	57.0	4168
LICT 020905-06	1	14	21.2	14.81	405	2691	-6	63.9	-5.9	49.8	3492
WSE 000715-00	2	766	22.8	9.18	1404	1630	-1	16.4	-6.4	58.2	2503
WSSS 030828-00	2	16	24.6	17.56	456	2136	-4	74.1	-3.4	45.6	4277
WSSS 000918-09	0	16	25.6	17.89	528	2223	-16	147.2	-4.6	46.0	4571
YPDN 020314-00	0	30	29.0	18.24	718	3121	-6	322.7	-3.4	42.0	4679
VECC 000722-00	0	6	25.2	19.54	276	1167	-1	489.6	-2.2	44.8	5171
YPDN 021104-12	2	30	29.6	18.11	764	3232	-2	40.3	-3.8	45.3	5017

TABLE 4. Largest and smallest values of spatial updraft maximum WMAX during 80-120 min, and brief description of storm type, for each storm case listed in Table 3.

Case	80-120 min WMAX values		Brief description of storm type
	Largest ($m\ s^{-1}$)	Smallest ($m\ s^{-1}$)	
ILX 960420-00	36.6	27.9	Splitting supercell, evolving to backbuilding multicell
ALB 950715-00	49.7	30.9	Backbuilding multicell
ILX 040714-00	64.5	40.1	Backbuilding multicell
OKX 050915-12	25.1	17.4	Complex multicell
ZBAA 050710-12	26.2	10.3	Backbuilding multicell
IAD 940501-00	22.2	13.8	Splitting supercell
11722 020716-12	29.1	24.6	Complex multicell
10393 020710-18	32.8	18.1	Complex multicell
11952 050731-12	25.3	15.1	Splitting supercell, evolving to backbuilding multicell
07145 970824-12	31.6	19.8	Complex multicell
10410 040717-12	25.6	15.2	Backbuilding multicell
TUS 980718-00	30.5	20.3	Complex multicell
BMX 980409-00	45.9	39.3	Splitting supercell
BNA 980416-18	27.1	20.5	Complex multicell
RKJJ 010714-12	17.1	11.3	Splitting supercell
FWD 010615-00	54.0	35.6	Backbuilding multicell
LGAT 020727-12	22.4	11.3	Complex multicell
ZGCS 040421-12	34.5	20.9	Splitting supercell, evolving to backbuilding multicell
LFME 030817-12	49.4	28.8	Complex multicell
40179 021016-00	50.5	39.0	Splitting supercell
16144 980630-12	39.3	20.1	Splitting supercell
LICT 020905-06	37.5	24.2	Complex multicell
WSE 000715-00	26.9	20.4	Supercell
WSSS 030828-00	28.4	13.6	Backbuilding multicell
WSSS 000918-09	14.9	6.0	Complex multicell
YPDN 020314-00	34.5	18.0	Complex multicell
VECC 000722-00	22.0	8.2	Backbuilding multicell
YPDN 021104-12	42.0	28.8	Backbuilding multicells

TABLE 5. Percentage partitionings of the 60-120 min time-averaged hydrometeor mass indices for each storm case listed in Table 3.

Case	Cloud Water	Cloud Ice	Rain	Snow	Graupel/ Hail	Total Ice	Total Liquid	Total Precipitation	Total Cloud	Frozen Precipitation
ILX 960420-00	12.3	5.9	19.2	17.8	44.7	68.4	31.6	81.8	18.2	62.5
ALB 950715-00	8.3	5.0	19.2	29.7	37.8	72.5	27.5	86.7	13.3	67.5
ILX 040714-00	6.3	5.4	16.7	18.4	53.2	77.0	23.0	88.3	11.7	71.6
OKX 050915-12	17.1	3.1	42.0	11.7	26.1	40.9	59.1	79.9	20.1	37.9
ZBAA 050710-12	16.7	4.3	29.3	18.4	31.3	54.1	45.9	79.0	21.0	49.7
IAD 940501-00	13.4	3.8	31.0	20.0	31.8	55.6	44.4	82.9	17.1	51.8
11722 020716-12	12.7	4.7	22.8	21.2	38.6	64.5	35.5	82.5	17.5	59.8
10393 020710-18	10.3	5.9	20.3	23.3	40.2	69.4	30.6	83.8	16.2	63.5
11952 050731-12	9.1	5.5	18.5	34.0	33.0	72.5	27.5	85.5	14.5	67.0
07145 970824-12	16.3	4.3	27.5	16.8	35.1	56.2	43.8	79.3	20.7	51.9
10410 040717-12	13.6	4.5	21.2	24.6	36.1	65.2	34.8	81.8	18.2	60.7
TUS 980718-00	12.2	7.3	13.5	26.6	40.4	74.3	25.7	80.5	19.5	67.0
BMX 980409-00	11.4	4.8	23.4	8.6	51.8	65.2	34.8	83.8	16.2	60.4
BNA 980416-18	15.0	4.1	23.4	15.8	41.8	61.6	38.4	80.9	19.1	57.5
RKJJ 010714-12	14.7	1.9	46.5	17.9	19.0	38.8	61.2	83.4	16.6	36.9
FWD 010615-00	7.6	5.5	20.4	22.4	44.1	72.0	28.0	87.0	13.0	66.5
LGAT 020727-12	14.7	4.3	30.7	21.1	29.1	54.6	45.4	81.0	19.0	50.2
ZGCS 040421-12	10.2	5.1	31.6	14.3	38.9	58.2	41.8	84.7	15.3	53.2
LFME 030817-12	6.9	4.9	19.3	20.2	48.6	73.8	26.2	88.2	11.8	68.9
40179 021016-00	6.9	4.5	19.7	13.8	55.2	73.4	26.6	88.6	11.4	68.9
16144 980630-12	5.8	4.7	23.5	21.0	45.0	70.7	29.3	89.5	10.5	66.0
LICT 020905-06	9.7	5.1	22.9	22.6	39.8	67.4	32.6	85.2	14.8	62.3
WSE 000715-00	8.5	6.5	14.3	20.3	50.4	77.1	22.9	85.0	15.0	70.6
WSSS 030828-00	18.6	2.3	45.0	13.3	20.7	36.4	63.6	79.0	21.0	34.1
WSSS 000918-09	24.0	1.3	37.6	18.5	18.6	38.4	61.6	74.7	25.3	37.1
YPDN 020314-00	33.1	2.0	38.3	12.5	14.1	28.6	71.4	64.9	35.1	26.6
VECC 000722-00	29.4	1.4	50.7	7.9	10.6	19.9	80.1	69.3	30.7	18.5
YPDN 021104-12	10.5	3.9	34.8	18.4	32.5	54.7	45.3	85.7	14.3	50.9

TABLE 6. Rankings of the time-averaged precipitation sources and sinks for 7 selected storm cases from the 28 listed in Table 3 (beginning).

	VECC 000722-00	YPDN 020314-00	40179 021016-00	WSSS 000918-09
RAIN SOURCES				
qracw	1	1	3	3
qrcnw	4	4	4	4
qsacw	6	6	6	6
qhmlr	2	3	1	1
qsmlr	5	5	5	5
qhshr	3	2	2	2
RAIN SINKS				
qiacr	3	3	3	3
qrfrz	5	5	5	5
qsacr	4	4	4	4
qrcev	2	2	2	2
qhacr	1	1	1	1
HAIL SOURCES				
qhcns	8	9	9	9
qraci	11	11	10	11
qiacr	4	4	4	4
qrfrz	10	10	11	10
qsacr	6	5	5	6
qracs	5	6	7	5
qhdpv	7	7	8	7
qhacr	1	1	1	1
qhacw	2	2	2	2
qhacs	3	3	3	3
qhaci	9	8	6	8
HAIL SINKS				
qhshr	2	1	2	2
qhmlr	1	2	1	1
qhsbv	3	3	3	3
SNOW SOURCES				
qsacw	1	2	2	2
qscni	8	8	9	8
qsaci	5	6	5	5
qisfi	2	1	1	1
qisfw	11	11	10	11

qraci	9	10	11	9
qiacr	4	3	3	4
qrfrz	10	9	7	10
qsacr	7	7	8	7
qsdpv	3	4	4	3
qracs	6	5	6	6
SNOW SINKS				
qhcns	4	4	4	4
qsmlr	3	3	3	3
qhacs	1	1	1	1
qssbv	2	2	2	2

TABLE 6 Rankings of the time-averaged precipitation sources and sinks for 7 selected storm cases from the 28 listed in Table 3 (concluded).

	ILX 040714-00	LGAT 020727-12	07145 970824-12
RAIN SOURCES			
qracw	3	3	3
qrcnw	4	5	4
qsacw	6	6	6
qhmlr	1	1	2
qsmlr	5	4	5
qhshr	2	2	1
RAIN SINKS			
qiacr	3	3	3
qrfrz	5	5	5
qsacr	4	4	4
qrcev	2	2	2
qhacr	1	1	1
HAIL SOURCES			
qhcns	9	9	9
qraci	10	10	10
qiacr	3	4	4
qrfrz	11	11	11
qsacr	5	5	5
qracs	8	6	6
qhdpv	7	7	7
qhacr	1	1	1
qhacw	2	2	2

qhacs	4	3	3
qhaci	6	8	8
HAIL SINKS			
qhshr	2	2	1
qhmlr	1	1	2
qhsbv	3	3	3
SNOW SOURCES			
qsacw	2	2	2
qscni	8	8	8
qsaci	5	5	5
qisfi	1	1	1
qisfw	10	10	11
qraci	11	9	10
qiacr	3	3	3
qrfrz	9	11	9
qsacr	7	7	7
qsdpv	4	4	4
qracs	6	6	6
SNOW SINKS			
qhcns	4	4	4
qsmlr	3	3	3
qhacs	1	1	1
qssbv	2	2	2

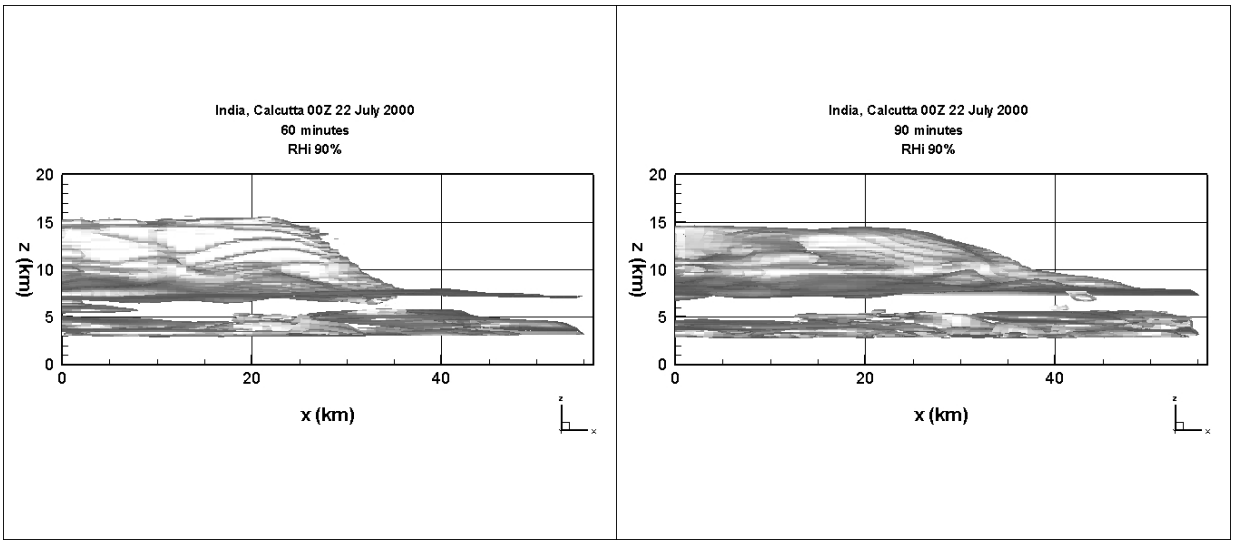

Figure 1. The approximate cloud boundary, defined by the isosurface of 90% relative humidity w.r.t. ice, for storm case VECC 000722-00 (Calcutta, India), looking north at 60 min (left panel) and 90 min (right panel).

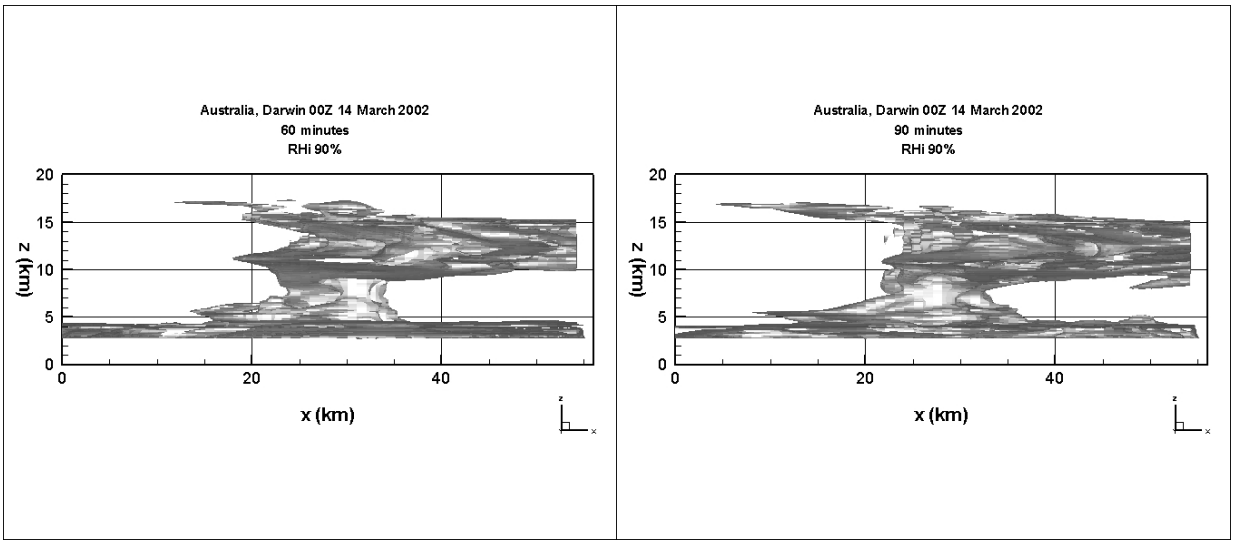

Figure 2. Same as Fig. 1, but for storm case YPDN 020314-00 (Darwin, Australia).

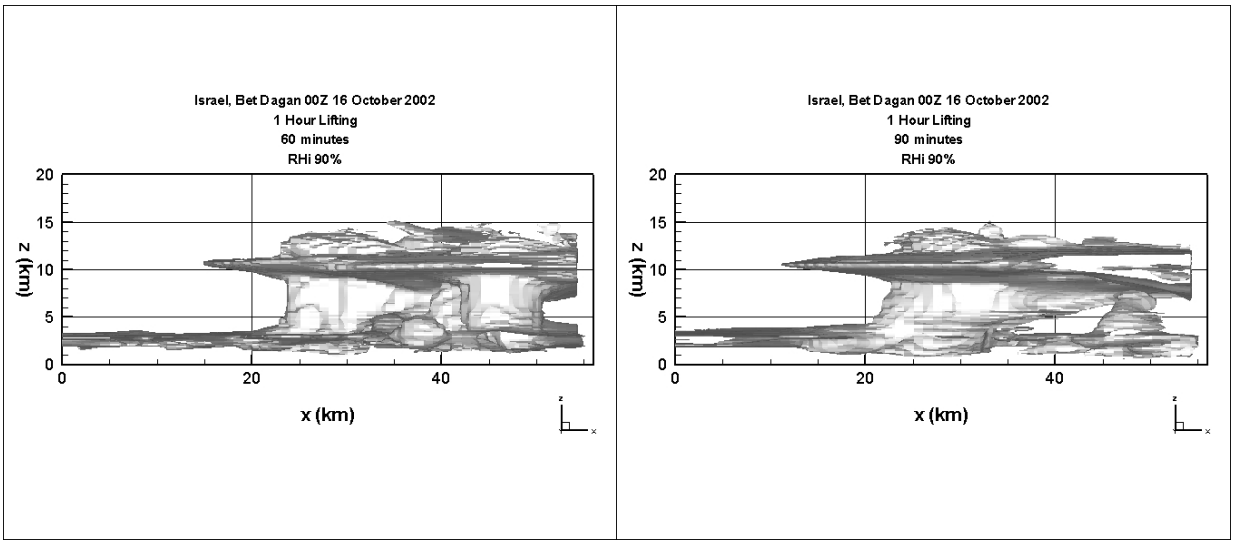

Figure 3. Same as Fig. 1, but for storm case 40179 021016-00 (Bet Dagan, Israel).

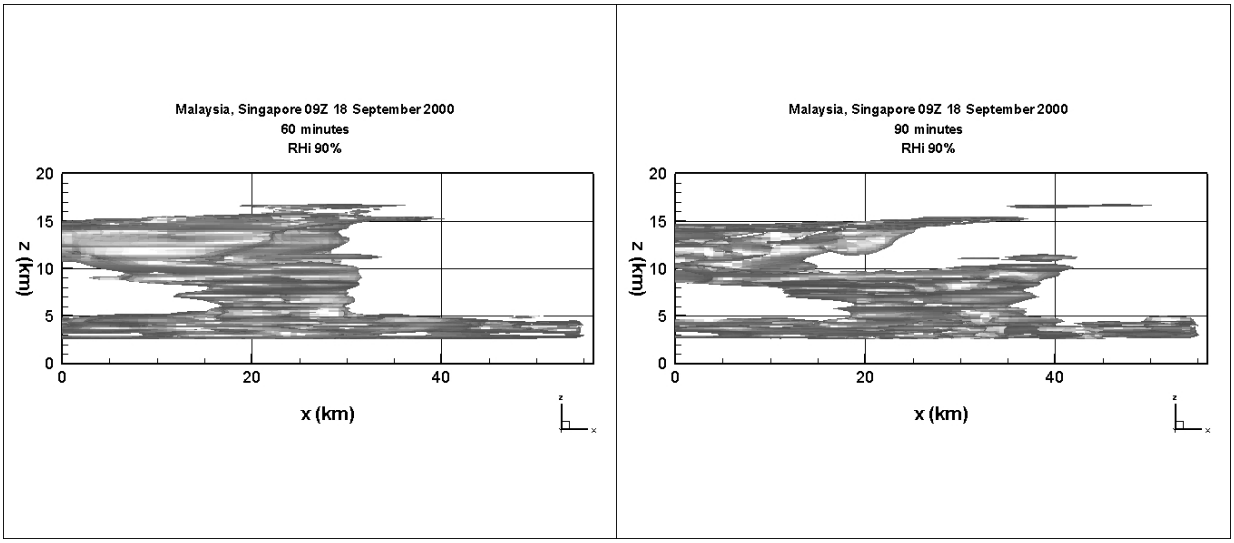

Figure 4. Same as Fig. 1, but for storm case WSSS 000918-09 (Singapore, Malaysia).

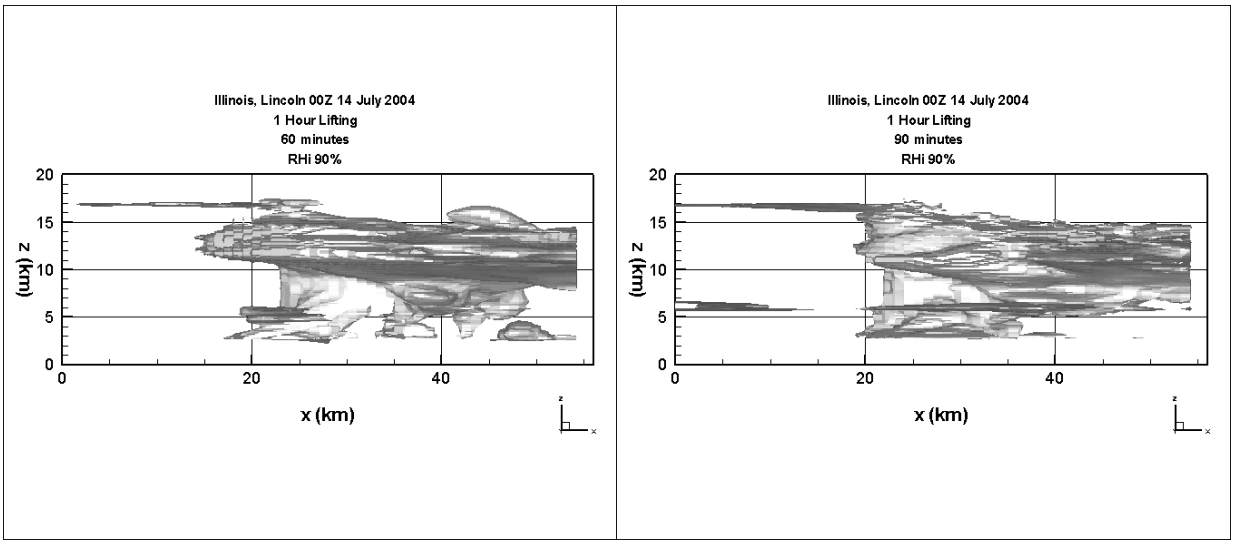

Figure 5. Same as Fig. 1, but for storm case ILX 040714-00 (Lincoln, IL).

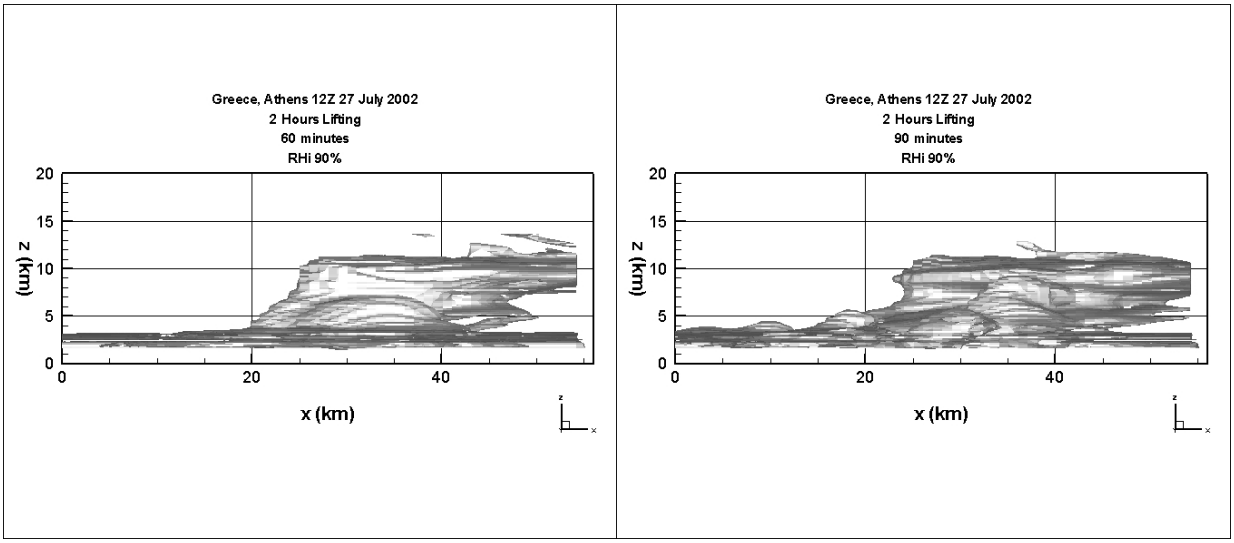

Figure 6. Same as Fig. 1, but for storm case LGAT 020727-12 (Athens, Greece).

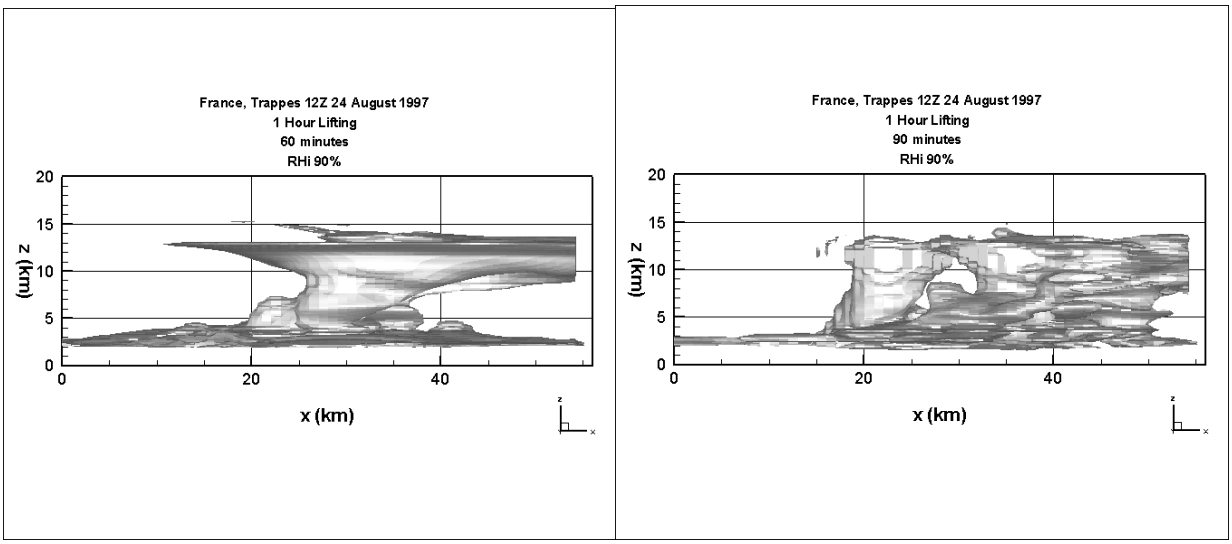

Figure 7. Same as Fig. 1, but for storm case 07145 970824-12 (Trappes, France).